Journal of Carcinogenesis
Covering Genesis to Therapeutics

Journal of Carcinogenesis, ISSN: 1477-3163
2025; Vol 24: Issue 4s, https://carcinogenesis.com/

Spatio-Temporal Graph Convolutional Network on Sequential Chest X-Rays for Early Bronchopulmonary Dysplasia Prediction

K. Akila[1], L.R.Aravind Babu[2]

[1]Research Scholar, Department of Computer and Information Science, Annamalai University, Chidambaram, Tamilnadu
Email ID: akilakrish227@gmail.com

[2]Assistant Professor, Department of Computer and Information Science, Annamalai University.

ABSTRACT

One of the most prevalent and harmful respiratory conditions in preterm infants is bronchopulmonary dysplasia (BPD), particularly those born very early and with extremely low birth weight. In the past, BPD was believed to be a chronic progressive lung disease that also affected the pulmonary parenchyma and vascular abnormalities. Children with BPD are much more likely to experience long-term cognitive dysfunction, cerebral palsy, speech impairment, pulmonary dysfunction, hearing and visual impairment, such as retinopathy of prematurity, and other conditions than children without BPD. Physicians used chest radiographs and their subjective judgment to diagnose BPD. Different subjective evaluations of BPD may result from physicians' varying clinical experiences and physical circumstances. In order to improve the quality of medical care and enable physicians to make more accurate and early diagnoses, a machine learning (ML)-based system is employed for the effective and efficient prediction of lung development in preterm newborns. This study aims to develop a Spatio-Temporal Graph Convolutional Network on Sequential Chest X-Rays for Early Bronchopulmonary Dysplasia Prediction **(**STGCN-CEBDP). At first, data preprocessing is used to pre-process the raw information from chest X-ray imaging. Next, DenseNet-3D is applied for the feature extraction process to capture both **spatial patterns** in chest X-ray sequences and **temporal changes** over time, which can enhance early BPD prediction. Following, STGCN is employed for the BPD prediction process. Finally, Whale Optimization Algorithm (WOA)-based hyperparameter tuning is conducted to enhance outcomes of accurate STGCN prediction. The simulation outcomes of the STGCN-CEBDP approach is tested on medical imaging database, and the experimental analysis demonstrate the enhancements of the STGCN-CEBDP method over other DL models.

Keywords: *Bronchopulmonary dysplasia**,** Machine learning, Chest X-Rays, Spatio-Temporal Graph Convolutional Network, Whale Optimization Algorithm)*

How to Cite: K. Akila, L.R.Aravind Babu, (2025) Spatio-Temporal Graph Convolutional Network on Sequential Chest X-Rays for Early Bronchopulmonary Dysplasia Prediction, *Journal of Carcinogenesis*, *Vol.24, No.4s*, 202-210

1. INTRODUCTION

In pediatrics, complications of preterm birth pose a serious health risk where premature babies are susceptible to both short-and long-term health complications due to underdeveloped organs, especially the lungs [1]. The most common cause of respiratory morbidity in preterm newborns is bronchopulmonary dysplasia (BPD), sometimes referred to as chronic lung disease [2]. One of the most frequent causes of morbidity and death in preterm newborns is BPD, which is brought on by lung injury that interferes with the development of the alveolar and pulmonary arteries. BPD is still the most frequent complication related to prematurity, and its prevalence is rising as a result of the higher survival rate of children born at extremely low gestational ages [3]. Usually, it is diagnosed in newborns with an oxygen need 28 days after birth, and the severity is assessed based on the degree of respiratory support needed at 36 weeks' post-menstrual age (PMA). BPD has been classified into 3 phases, namely mild, moderate, and severe cases. The pathophysiology of BPD has changed over the last few decades, evolving from high oxygen levels to a complex illness including both prenatal and postnatal causes and pulmonary lesions to mechanical ventilation [4]. When chorioamnionitis occurs during pregnancy, premature infants that have less pulmonary vascular development are more likely to have BPD. Clinical factors that have been extensively examined include postnatal infections, necrotizing enterocolonitis (NEC), patent ductus arteriosus (PDA), gender, birth

weight, gestational age (GA), and the need for mechanical ventilation or oxygen administration. With almost 15 million premature babies born each year, preterm BPD birth continues to contribute significantly to the global burden of disease [5].

Furthermore [6], a variety of complications are more likely to occur in infants with severe BPD, necessitating multidisciplinary cooperation both post-discharge home treatment and hospitalisation. Therefore, earlier diagnosis, individualised management, and precise prevention have become the keystones of therapeutic care of preterm children with BPD, which improves patient survival and prognosis [7]. Although BPD has an operational clinical description, it is difficult to make an accurate forecast because of its diverse clinical phenotypes and endotypes. Monitoring a premature baby's oxygen needs with tools like pulse oximetry, chest X-rays to visualize lung changes, blood tests to measure oxygen levels, and occasionally an echocardiogram to rule out heart defects as a contributing factor to BPD early diagnosis [8]. A diagnosis is typically made if a baby needs supplemental oxygen for a long time after birth, especially after 28 days, and exhibits distinctive lung changes on imaging.

To better understand, diagnose, and manage BPD in patients [9], researchers have turned to computational tools, such as artificial intelligence (AI) and machine learning (ML). By analyzing chest X-ray images, predictive analytics can improve BPD management through statistical and ML techniques to predict individual patient outcomes and increase the diagnostic accuracy of BPD in preterm newborns. To learn how input features (such as clinical data) relate to known outcomes, the algorithms are trained on labeled datasets. On the other hand, it provides insights into the development of clinical phenotypes by identifying patterns or clusters in data without the need for predetermined labels [10].

This study aims to develop a Spatio-Temporal Graph Convolutional Network on Sequential Chest X-Rays for Early Bronchopulmonary Dysplasia Prediction **(**STGCN-CEBDP). At first, data preprocessing is used to pre-process the raw information from chest X-ray imaging. Next, DenseNet-3D is applied for the feature extraction process to capture both spatial patterns in chest X-ray sequences and temporal changes over time, which can enhance early BPD prediction. Following, STGCN is employed for the BPD prediction process. Finally, Whale Optimization Algorithm (WOA)-based hyperparameter tuning is conducted to enhance outcomes of accurate STGCN prediction. The simulation outcomes of the STGCN-CEBDP approach is tested on a medical imaging database, and the experimental outcome demonstrate the enhancements of the STGCN-CEBDP technique over other DL models.

2. RELATED WORKS

He et al. [11] developed ML prediction mechanisms for BPD severity based on selected clinical factors in a Chinese population. During the early postnatal, maternal, and delivery phases, we gathered their clinical data. Using ordinal and univariate logistic regression analyses, risk factors were chosen. In the end, 471 patients were included (279 mild, 147 intermediate, and 45 severe instances). The following characteristics were independent risk factors for the severity of BPD on ordinal logistic regression. The models can help forecast the severity of BPD in the Chinese population and perform well.

Chou et al. [12] employed AI techniques to assist medical doctors accurately in quickly and reliably diagnosing BPD in premature infants. Two datasets are used in this retrospective study: a BPD prediction dataset with 1021 preterm infant chest radiographs and a lung region segmentation dataset with 1491 infant chest radiographs. To increase the performance, TL of a previously trained ML technique was used for image fusion for BPD prediction and lung region segmentation. Using TL, the lung segmentation model achieves a dice score of 0.960 for preterm newborns who are ≤ 168 hours postnatal. The BPD prediction model consistently performed well for chest radiographs taken between 25 and 168 hours after birth, as well as those taken at less than 24 hours. Its diagnostic performance was superior to that of other techniques.

Hwang et al. [13] present an improved ML-based prediction technique for BPD and its severity through a two-stage method in conjunction with the duration of respiratory support (RSd) using postnatal and early prenatal variables from a nationwide very low birth weight (VLBW) infant cohort. Forty-five clinical factors from prenatal and early perinatal care were chosen in this study. Modeling and a stepwise approach were conducted using a MLP-based analysis, which was newly proposed to predict disorders in preterm newborns. We also developed new BPD prediction models (PMbpd) and used a complementary MLP network. Each variable's contribution was determined using the Shapley approach. The study demonstrated important clinical factors for the highly accurate earlier prediction of BPD and its severity.

Leigh et al. [14] present an ML-based survival prediction tool devoid of BPD based on the idea that BPD has a developmental foundation. Initial model development was done using datasets that included perinatal variables and early postnatal respiratory support. The two models were then combined using LR to create a final ensemble model. The study contained data from 689 newborns. Data from 80% of newborns were chosen at random for model building, while the remaining 20% were employed for validation. The receiver operating characteristics were used to evaluate the final model's performance; the results for the training and validation datasets were 0.921, correspondingly. According to simulation results, extubating to CPAP improves BPD-free survival more than NIPPV. A successful extubation can also

be characterized by the absence of reintubation for nine days after the initial extubation.

3. THE PROPOSED MODEL

In this work, we present an STGCN-CEBDP model. At first, data preprocessing is used to pre-process the raw information from chest X-ray imaging. Next, DenseNet-3D is applied for the feature extraction process to capture both spatial patterns in chest X-ray sequences and temporal changes over time, which can enhance early BPD prediction. Following, STGCN is employed for the BPD prediction process. Finally, Whale Optimization Algorithm (WOA)-based hyperparameter tuning is conducted to enhance outcomes of accurate STGCN prediction. Figure 1 demonstrates the overall architecture of the STGCN-CEBDP model

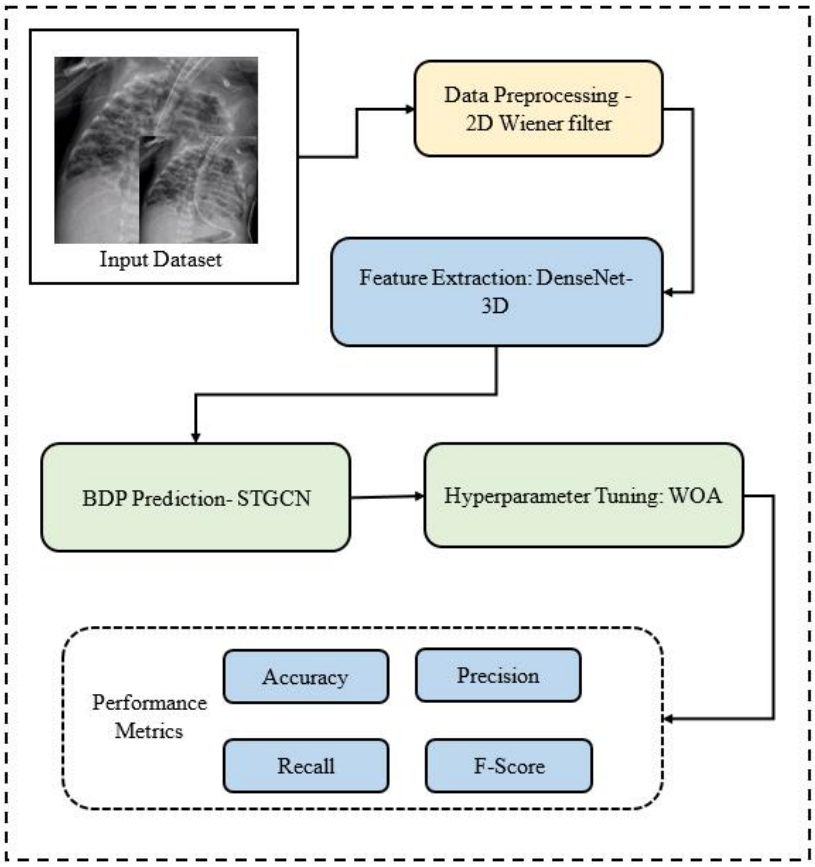

Figure 1. Overall architecture of the STGCN-CEBDP model

3.1. Image Pre-Processing

At first, data preprocessing is used to pre-process the raw information from chest X-ray imaging [15]. One of the most well-known linear filters for eliminating noise and enhancing deteriorated image quality is the two-dimensional (2D) Wiener filter (WF). Eq. (1) provides a mathematical expression for the degraded image $g(x,]^{f})$:

$$g(x_p y) = f(x,y) \otimes h(x,y) + \eta(x,]^{\Gamma}) \quad (1)$$

In this case, the original (ideal) picture is represented by $f(x,]^{\Gamma})$, and the pixels of the degradation function $h(x,y)$, is represented by. The original image is recovered by the deconvolution process. To determine the error between two images, the WF, a deconvolution filter, is used to estimate the number of the ideal (original) picture.

$$error^2 = \varepsilon\{(\# - f)^2\} \quad (2)$$

Where the expected value of the argument is ε. The Fourier transform applies the WF. The degraded image g_{xy} is transformed into the Discrete Founer Transform to yield G_{uv}. The original image S spectrum is calculated using the following equation:

$$S_{utJ} = W_{uv} * G_{utJ} \quad (3)$$

In the frequency domain, the Wiener filter (W) can be evaluated by:

$$W_{\mathfrak{U}tJ} = \frac{\mathbb{H}^*_{uv}}{E^*_{1A\eta}\cdot\mathbb{H}_{uv}+\zeta\frac{1}{SN\mathbb{R}})} \quad (4)$$

In Eq. (4), SNR stands for Signal-to-Noise Ratio, H^*_{uv} indicates the conjugate complex of H_{uv}, and G_{utJ} is the input image's Fourier transform. $1[S\mathbb{NR}$ is Signal Noise Ratio in reverse. The range of $1[S\mathbb{NR}$ values is [0.0001-0.01], which is a constant number.

3.2. DenseNet-3D Based Feature Extraction

In order to improve early BPD prediction [16], DenseNet-3D is used for the feature extraction method to capture both temporal changes over time and spatial patterns in chest X-ray sequences. The process of identifying and extracting relevant properties or features of an image is known as feature extraction. It is a crucial stage in image analysis because it helps reduce the image into a compact format that can be processed quickly for a classification task or other purposes. As a variant of a convolutional neural network (CNN), DenseNet features dense connections between layers within dense blocks and is made up of four dense blocks. Because of its many benefits, we decided to use DenseNet as the foundational model in our investigation. Initially, over-fitting may be minimized by DenseNet. Since DenseNet uses less than half of ResNet's parameters, it is computationally effective. Our study focused on 3D chest X-ray sequences [17], even though DenseNet was first created for two-dimensional scans. Since the majority of medicinal images are 3D, we created a 3D-DenseNet with 3D versions of the kernels for all the convolutional and pooling layers. Each layer of the suggested 3D DenseNet model employed the ReLu as an activation function, and the final layer of our network applied the softmax function to determine the probability for every sample. By inflating its filters and pooling kernels, DenseNet-2D was converted to DenseNet-3D in order to extract temporal and spatial information from X-ray imaging.

3.3. BPD Prediction using STGCN

Following, STGCN is used in the BPD prediction procedure. A robust deep learning system called STGCN was created specially to handle complex spatiotemporal data and its connections [18]. It effectively captures complex patterns and correlations in the data by fusing the features of Graph Neural Networks with time series models. This method works especially well for processing spatiotemporal information in imaging data. It models the timing and structure of CXR images at the same time, improving the accuracy of BDP predictions. Environmental monitoring, healthcare, traffic prediction, demand forecast, and energy production are prominent uses for ST-GCN model. Using spatiotemporal GCN methods, this study presents a modeling framework based on spatiotemporal data, called the ST-GCN model, to thoroughly analyze and forecast interchange patterns.

In order to represent the crucial dimensions for training STGCN, a GCN-based model, a crucial first step in this study was creating graphs. Graph data is used for both training and analysis in GCN-based algorithms. We used a technique to generate these graph data, assigning the extracted data value inside the graph to the average value of the point data that shared the same link index. Each link's connection information was identified as the graph's edge information [19]. A graph representation of spatiotemporal properties was the result of this procedure. Consider a graph as $\mathcal{G}(\mathcal{V},\mathcal{E})$ with edges $\mathcal{E}$ and vertices V. For $i \in \{1,2,\ldots,N\}$, where the total number of nodes is denoted as N, f_i represents a vertex feature of the length of d^0. Where $e_{ij} \geq 0$ and $i, j \in \{1,2,\ldots,N\}$, e_{ij} is expressed as edge weights.

$$H^{l+1} = g(H^l, A) = \sigma\left(\widehat{D}\widehat{A}\widehat{D}H^lW^l\right) \quad (5)$$

In Eq. (5), the $d^l \times d^{l+1}$ and $N \times d^l$ weight and input matrices of the l^{th} layer is represented by W^l and H^l, correspondingly.

$$\widehat{A} = I + A \quad (6)$$

In Eq. (6), the diagonal node degree matrix of $\widehat{A}$ is referred to as $A = [e_{i,j}], \widehat{D}$.

The original purpose of STGCN was BDP diagnosis [20]. We use frame-based graphs that are extracted by situation recognition to apply STGCN for the segmentation of image sequences. Two key differences in our STG allow for additional application requirements. Initially, the CXR served as the basis for the original STGCN, with spatial edges signifying the physical link between joints and graph nodes representing actual joints. Rather, we build our spatial graph using CXR interactions, where nodes stand in for actors, objects, scenes, and actions, and edges show their functional (e.g., role) and/or spatial (e.g., next to) ties. Second, the original STGCN reduces to a fixed and grid-like connectivity since it only links physical joints of the similar type over successive time stamps. The temporal GCN consequently deteriorates to conventional convolution. Our graph permits random temporal connections to accommodate flexible setups and frequently occurring graph deformation in complicated activities (e.g., missed detections, strong occlusions, emerging/disappearing objects, etc. Let the spatial and temporal adjacency matrices be represented by A_s and A_t, correspondingly. The following is a mathematical representation of our suggested STGCN operation:

$$H^{l+1} = g_t(H^l_s, A_t) = \sigma(\widehat{D}\widehat{A}\widehat{D}H^l_sW^l_t) \quad (7)$$

$$H_s^l = g_s(H^l, A_s) = \widehat{D}\widehat{A}\widehat{D}H^l W_s^l \quad (8)$$

In the Equations, the spatial and temporal weight metrics of the l^{th} convolution layers are denoted by W_s^l and W_t^l, correspondingly. The STGCN is made up of a full connection layer and several ST-Conv blocks. By performing convolution along the time axis, the model captures the temporal dynamic characteristics. The following is an expression for the gated sequential convolution process used to handle the time frame at t:

$$H^{l+1} = g(H^l, A_s) = \sigma\left(\widehat{D}\widehat{A}\widehat{D}H^l W_s^l W_t^l\right) \quad (9)$$

The performance of a prediction task is largely determined by an adjacency matrix, which reflects the spatial dependency or graph in STGCN. According to the results, STGCN consistently outperformed other algorithms and was able to capture the spatialtemporal correlations of the traffic network.

3.4. WOA Hyperparameter Tuning

Finally, Whale Optimization Algorithm (WOA)-based hyperparameter tuning is conducted to enhancing outcomes of accurate STGCN prediction [21]. WOA is a new swarm intelligence algorithm that draws inspiration from nature to more efficiently quickly address the optimization problems. WOA is based on the hunting strategy of humpback whales. When whales hunt in groups of small fish, they encircle and capture their prey using the bubble-net technique. X^* is the best whale position in WOA, and the other whales adjust their positions based on it. Whales in WOA engage in three behaviors: encircling prey, bubble-net attacking (exploitation), and looking for prey (exploration).

Encircling prey: Surrounding the prey is the first stage of the hunting process. Whales can locate their target and start to encircle them. Consequently, in WOA, the best whale X^* at the moment is regarded as prey or as being near prey. Eqs. (6) and (7) are used by all other whales to update their location according to the X^*:

$$D = |C \times X^*(t) - X(t)| \quad (10)$$

$$X(t+1) = X^*(t) - A \times D \quad (11)$$

Here, D indicates the estimated distance between the whale $X(t)$ and the prey $X^*(t)$, and t shows the iteration timer.

$$A = 2 \times a \times r - a(t) \quad (12)$$

$$C = 2 \times r \quad (13)$$

Where r is a random number in $[0,1]$ and the value of a is linearly reduced from 2 to 0 during the iterations.

Bubble-net attacking: Whales use a spiral updating position or a diminishing encircling strategy as they spin around their prey. This behavior can be expressed by.

$$X(t+1) = \begin{cases} X^*(t) - A \times D & if\ p < 0.5 \\ D' \times e^{bl} \times \cos(2 \times \pi \times l) + X^*(t) & if\ p \geq 0.5 \end{cases} \quad (14)$$

In Eq. (14), the probability of updating whale positions using a spiral updating location (if $p > 0.5$) or a shrinking encircling strategy (if $p < 0.5$) is indicated by p, a random value within $[0,1]$. Throughout the iterations, A random variable in $[-a, a]$, is gradually reduced from 2 to 0. During the spiral updating position, l is a random number in $[1,1]$, b is a constant that defines the spiral movement shape, and D' is the distance between the current whale X and the prey X^*.

Searching for prey: Whales search the entire search range to locate new prey. When vector $A's$ absolute value is larger than or equivalent to 1, then it is completed; and it is considered exploration; otherwise, it is considered exploitation. The whales update their position with respect to a random whale X_{rand} during the exploration phase rather than the best whale X^*, which is determined using the following equations:

$$D = |C \times X_{rand} - X(t)| \quad (15)$$

$$X(t+1) = X_{rand} - A \times D \quad (16)$$

Here, X_{rand} refers to a whale chosen at random from the existing population.

To achieve better classification performance, the WHO approach calculates a fitness function. It chooses a positive number to indicate which of the potential solutions performs better. According to Eq. (17), the fitness function in this study is the minimization of the classification error rate.

$$fitness(x_i) = ClassifierErrorRate(x_i) = \frac{no.\ of\ misclassified\ samples}{Total\ no.\ of\ samples} * 100 \quad (17)$$

4. EXPERIMENTAL ANALYSIS

In this section, the simulation outcomes of the STGCN-CEBDP method are examined utilizing Kaggle dataset, which contains 37260 samples with 5 class labels shown in Table 1. Figure. 2 demonstrates the BPD outcome of STGCN-CEBDP technique.

Table 1 Details on Dataset

Class	**No. of Count**
Mild	2445
Moderate	6222
Severe	873
BDP	908
Normal	26812
Total Count	**37260**

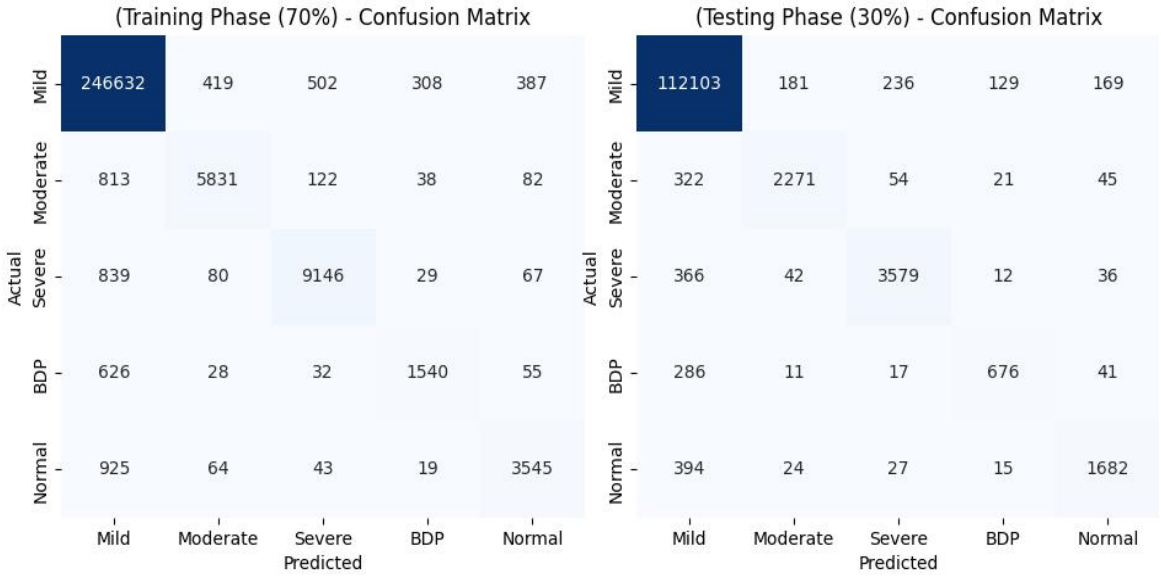

Figure 2 Confusion matrix of STGCN-CEBDP technique with 70%TRPH and 30%TSPH

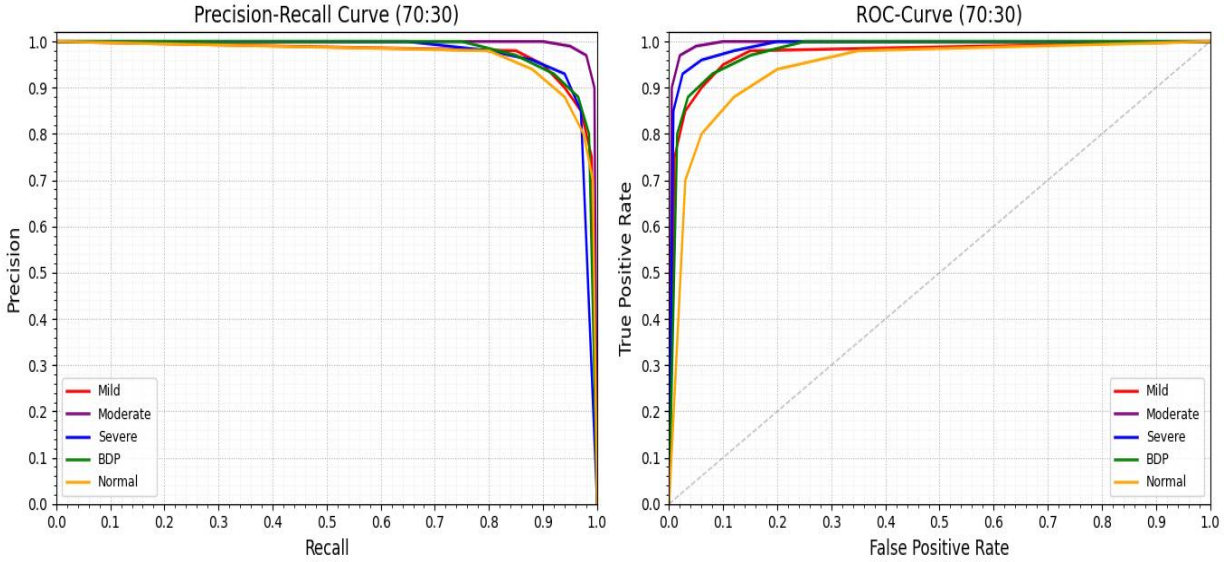

Figure. 3. PR and ROC curve of STGCN-CEBDP technique under 70:30 of TRPH/TSPH

The findings confirm that the STGCN-CEBDP method under 70%of TRPH/30%ofTSPH reliably accomplishes higher PR values across each class regarding the PR curve shown in Figure. 3. These outcomes underscore the model's effective capability for distinguishing between numerous classes, emphasizing its efficiency in identifying classes. Furthermore, ROC curves generated by the STGCN-CEBDP approach on 70:30 of TRPH/TSPH, demonstrating its capability to differentiate between classes. This provides valuable insight into how the trade-off between FPR and TPR differs across several thresholds and epochs. The outcomes highlight the model's classification performance on different classes, emphasizing its efficiency in prediction outcomes is illustrated in Table 2 and Figure 4.

Table 2 Prediction analysis of STGCN-CEBDP technique on 70:30 of TRPH/TSPH

Class	$Accu_y$	$Prec_n$	$Reca_l$	F_{score}
TRPH (70%)				
Mild	98.50	95.34	95.40	95.37
Moderate	97.49	97.23	97.39	97.31
Severe	96.60	86.95	95.85	91.19
BDP	98.64	88.17	94.02	90.47
Normal	99.12	99.69	99.10	99.40
Average	**98.07**	**93.45**	**96.33**	**94.75**
TSPH (30%)				
Mild	98.54	95.43	96.20	97.81
Moderate	97.58	97.47	97.72	96.60
Severe	98.51	85.58	96.56	89.85
BDP	97.70	90.19	99.12	92.52
Normal	98.96	99.64	98.94	95.29
Average	**97.32**	**93.62**	**97.70**	**93.52**

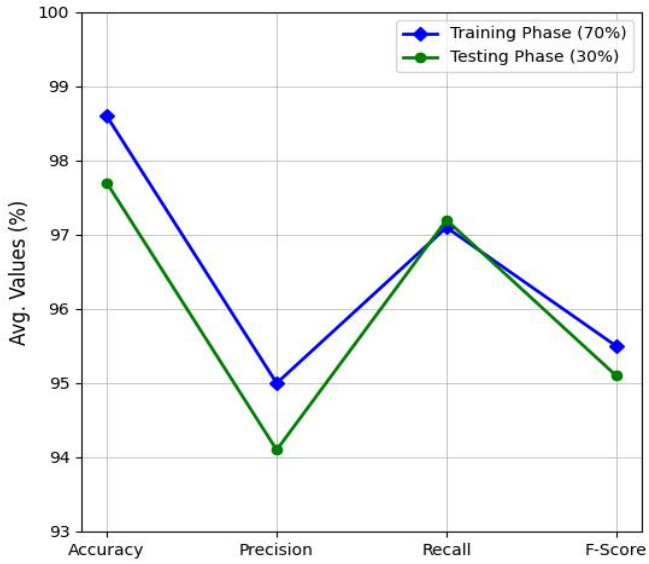

Figure. 4. Average of STGCN-CEBDP method on 70%TRPH and 30%TSPH

To determine the superior performance of the STGCN-CEBDP method, a comparison analysis is made in Table 4 and Figure 5. The outcomes demonstrated that the STGCN-CEBDP technique have shown higher prediction results. In the meantime, the SVM, ResNet-50, AlexNet and BiLSTM techniques have tried to accomplish somewhat closer prediction results.

Table 4 Comparative outcome of STGCN-CEBDP approach with other techniques

Approaches	$Accu_y$	$Prec_n$	$Reca_l$	F_{score}
STGCN-CEBDP	98.82	98.87	97.27	97.07
SVM	96.74	97.72	94.50	97.11
ResNet-50	94.13	96.42	96.98	97.70
AlexNet	95.96	98.18	95.46	97.32
BiLSTM	96.13	95.26	98.34	97.80

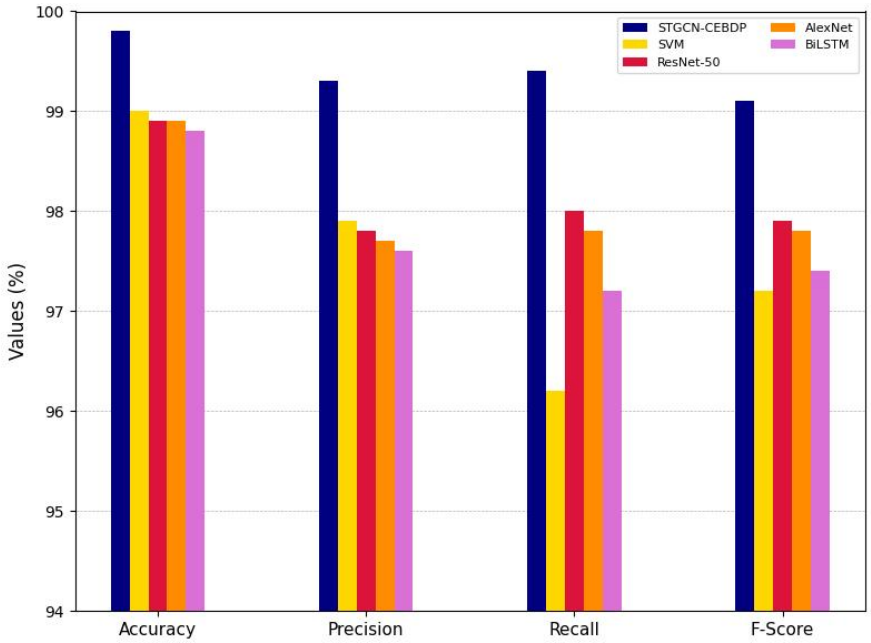

Figure. 5. Comparative outcome of STGCN-CEBDP technique with other models

5. CONCLUSION

In this study, we present a Spatio-Temporal Graph Convolutional Network on Sequential Chest X-Rays for Early Bronchopulmonary Dysplasia Prediction (STGCN-CEBDP). At first, data preprocessing is used to pre-process the raw information from chest X-ray imaging. Next, DenseNet-3D is applied for the feature extraction process to capture both spatial patterns in chest X-ray sequences and temporal changes over time, which can enhance early BPD prediction. Following, STGCN is employed for the BPD prediction process. Finally, WOA-based hyperparameter tuning is conducted to enhance outcomes of accurate STGCN prediction. The simulation outcomes of the STGCN-CEBDP method is tested on a medical imaging database, and the experimental outcomes demonstrate the enhancements of the STGCN-CEBDP method over other DL models.

REFERENCES

[1] De Rose, D.U., Liotto, N., Maggiora, E., Bini, P., Costa, S., Cresi, F., Morlacchi, L., Spinedi, S.F., Gizzi, C., Maggio, L. and Orfeo, L., 2025. Preventing Bronchopulmonary Dysplasia Through Nutrition in Preterm Infants: A Systematic Review of the Literature. Nutrition Reviews, p.nuaf110.

[2] Baud, O., Lehert, P. and PREMILOC study group, 2025. Bronchopulmonary dysplasia to predict neurodevelopmental impairment in infants born extremely preterm. Pediatric Research, 97(7), pp.2436-2442.

[3] Siffel, C., Kistler, K.D., Lewis, J.F. and Sarda, S.P., 2021. Global incidence of bronchopulmonary dysplasia among extremely preterm infants: a systematic literature review. The Journal of Maternal-Fetal & Neonatal Medicine, 34(11), pp.1721-1731.

[4] Gallini, F., Coppola, M., De Rose, D.U., Maggio, L., Arena, R., Romano, V., Cota, F., Ricci, D., Romeo, D.M., Mercuri, E.M. and Vento, G., 2021. Neurodevelopmental outcomes in very preterm infants: The role of severity of Bronchopulmonary Dysplasia. Early human development, 152, p.105275.

[5] Jensen, E.A., Whyte, R.K., Schmidt, B., Bassler, D., Vain, N.E. and Roberts, R.S., 2021. Association between intermittent hypoxemia and severe bronchopulmonary dysplasia in preterm infants. American journal of respiratory and critical care medicine, 204(10), pp.1192-1199.

[6] Qu, Y., Guo, S., Liu, Y., Wang, G. and Wu, H., 2021. Association between probiotics and bronchopulmonary dysplasia in preterm infants. Scientific Reports, 11(1), p.17060.

[7] Shirazi, S.P., Negretti, N.M., Jetter, C.S., Sharkey, A.L., Garg, S., Kapp, M.E., Wilkins, D., Fortier, G., Mallapragada, S., Banovich, N.E. and Eldredge, L.C., 2025. Bronchopulmonary dysplasia with pulmonary hypertension associates with semaphorin signaling loss and functionally decreased FOXF1 expression. Nature Communications, 16(1), p.5004.

[8] Talebi, H., Dastgheib, S.A., Vafapour, M., Bahrami, R., Golshan-Tafti, M., Danaei, M., Azizi, S., Shahbazi,

A., Pourkazemi, M., Yeganegi, M. and Shiri, A., 2025. Advancements in biomarkers and machine learning for predicting of bronchopulmonary dysplasia and neonatal respiratory distress syndrome in preterm infants. Frontiers in Pediatrics, 13, p.1521668.

[9] Choi, H.J., Lee, G., Shin, S.H., Lee, S.M., Lee, H.C., Sohn, J.A., Lee, J.A. and Kim, H.S., 2025. Development and external validation of a machine learning model to predict bronchopulmonary dysplasia using dynamic factors. Scientific Reports, 15(1), p.13620.

[10] Jha, T., Suhail, S., Northcote, J. and Moreira, A.G., 2025. Artificial Intelligence in Bronchopulmonary Dysplasia: A Review of the Literature. Information, 16(4), p.262.

[11] He, W., Zhang, L., Feng, R., Fang, W.H., Cao, Y., Sun, S.Q., Shi, P., Zhou, J.G., Tang, L.F., Zhang, X.B. and Qi, Y.Y., 2023. Risk factors and machine learning prediction models for bronchopulmonary dysplasia severity in the Chinese population. World Journal of Pediatrics, 19(6), pp.568-576.

[12] Chou, H.Y., Lin, Y.C., Hsieh, S.Y., Chou, H.H., Lai, C.S., Wang, B. and Tsai, Y.S., 2024. Deep learning model for prediction of bronchopulmonary dysplasia in preterm infants using chest radiographs. Journal of Imaging Informatics in Medicine, 37(5), pp.2063-2073.

[13] Hwang, J.K., Kim, D.H., Na, J.Y., Son, J., Oh, Y.J., Jung, D., Kim, C.R., Kim, T.H. and Park, H.K., 2023. Two-stage learning-based prediction of bronchopulmonary dysplasia in very low birth weight infants: a nationwide cohort study. Frontiers in Pediatrics, 11, p.1155921.

[14] Leigh, R.M., Pham, A., Rao, S.S., Vora, F.M., Hou, G., Kent, C., Rodriguez, A., Narang, A., Tan, J.B. and Chou, F.S., 2022. Machine learning for prediction of bronchopulmonary dysplasia-free survival among very preterm infants. BMC pediatrics, 22(1), p.542.

[15] Habeeb, N.J., 2023. Medical image denoising with wiener filter and high boost filtering. Iraqi Journal of Science, pp.3123-3135.

[16] Chambi, J.L.S., Cáceres, J.C.G. and Castañón, C.A.B., 2022, November. Densenet 3d for violent action recognition in surveillance video sequences. In 2022 41st International Conference of the Chilean Computer Science Society (SCCC) (pp. 1-8). IEEE.

[17] Li, G. and Ye, M., 2025. Dgcnet: An efficient 3d-densenet based on dynamic group convolution for hyperspectral remote sensing image classification. Spectroscopy Letters, pp.1-14.

[18] Qiao, Q., Xu, Z., Ren, C., Yunusa-Kaltungo, A. and Cheung, C., 2025. Building energy consumption prediction for campus accommodation buildings based on spatial temporal graph convolution networks. Procedia CIRP, 135, pp.498-502.

[19] Jeon, S.B. and Jeong, M.H., 2024. Integrating Spatio-Temporal Graph Convolutional Networks with Convolutional Neural Networks for Predicting Short-Term Traffic Speed in Urban Road Networks. Applied Sciences (2076-3417), 14(14).

[20] Lin, Z., 2025. Optimizing Kernel Extreme Learning Machine based on a Enhanced Adaptive Whale Optimization Algorithm for classification task. PloS one, 20(1), p.e0309741.

[21] Zhou, Y. and Hao, Z., 2025. Multi-strategy improved whale optimization algorithm and its engineering applications. Biomimetics, 10(1), p.47.